Advances in Science and Technology Vol. 68 (2010) pp 13-22

doi:10.4028/www.scientific.net/AST.68.13

Characterization of microstructure and crystallographic texture of silicate and phyllosilicate ceramics

Chateigner Daniel[1, a], Blanchart Philippe[2,b], Deniel Sarah[2,c], Lutterotti Luca[3,d], Wenk Hans-Rudolf[4,e]

[1]Lab. CRISMAT-ENSICAEN and IUT-Caen, Université de Caen Basse-Normandie, 6, Bd. M. Juin, 14050 Caen, France

[2]Lab. GEMH-ENSCI, 47-73, Av. A. Thomas, 87065 Limoges, France

[3]Dept. Materials Engineering, University of Trento, via Mesiano 77, 38123 Trento, Italy

[4]Dept. Earth and Planetary Science, University of California, Berkeley, California 94720, USA

[a]daniel.chateigner@ensicaen.fr, [b]philippe.blanchart@unilim.fr, [c]sarah.ensci@laposte.net, [d]luca.lutterotti@ing.unitn.it, [d]wenk@berkeley.edu

Keywords: Combined Analysis, Mullite, Phyllosilicate, Montmorillonite, turbostratic.

Abstract. We illustrate the x-ray Combined Analysis approach capabilities in characterizing silicates and phyllosilicates for samples exhibiting crystallographic textures. Two mullite composite ceramics, one elaborated under uniaxial pressure the other under centrifugation, and one uniaxially pressed montmorillonite aggregate, are studied in terms of texture, cell parameters and phase contents. Several weak texture components are present in the mullite samples, combinations of planar- and fibre-like textures. The methodology is able to take account of the amorphous silica-like matrix of the composite, and cell parameters and structure of mullite correspond to the commonly modelled used for this phase. The montmorillonite turbostratic phase is correctly reproduced with its fibre texture, eventhough minor phases are also present and modelled in the aggregate.

Introduction

Ceramics with an organized microstructure offer potentialities in obtaining specific mechanical behaviours, compared to monolithic compounds. For instance [1] alumina/alumina laminar composites with alternatively oriented crystallites in layers exhibit high bending and anisotropic strength. Work of fracture also can be improved by deflecting cracks at alumina interphase layers in oxide–oxide laminated composites with aluminum phosphate and alumina platelets [2]. Some ceramic processing techniques are able to spatially control the microstructure and induce the development of organized microstructures during sintering, in which morphology, periodicity, and connectivity of crystals are very important for mechanical improvements. In clay-derived ceramics, mullite formation undergoes various formation schemes depending of the precursor clay minerals [3], and resulting in different mullite stoichiometry, crystal sizes, and quantity [4, 5], with however acicular-like crystal shapes as a commonly obtained characteristic. Temperature is another influencing factor on mullite crystallisation [6]. Several interpretations of improved mechanical behaviour in mullite composites have been elaborated [7, 8, 9]. In organized ceramics with oriented microstructures, the degree of orientation can be achieved using large muscovite flakes, or by centrifugation and annealing of kaolin suspensions. In the former case, during the thermal cycle for sintering, the structural characteristics of muscovite are maintained, and the residual structural order of high temperature muscovite favours the epitaxial growth of mullite crystals. In this procedure the occurrence of a small quantity of liquid highly favours the mullite formation at a moderate temperature, typically below 1200°C. Crystal growth can be favoured by formation of a transient liquid phase at interfaces, for instance by adding Bi^{3+} cations [10]. However, whatever the orientation procedure, quantifying the texture quantitatively is often a problem in such ceramic

materials, mainly due to the presence of amorphous phases. In turbostratically disordered phyllosilicate samples, the main difficulty to probe texture quantitatively, is to be able to refine a model that gives a satisfactory fit of the experimental diffraction data, because these latter exhibit large "hk" scattering bands. Using a Rietveld compatible approach [11] is a way to incorporate the turbostratic disorder in the Combined Analysis method.

In this work we illustrate the crystallographic texture investigation of two mullite composite ceramics obtained by centrifugation and unidirectional pressing, and of a unidirectionally pressed turbostratic montmorillonite aggregate, with the help of the so-called Combined Analysis.

Experimental

Materials. Mullite ceramic samples were prepared using either uniaxial or centrifugation pressures. For the centrifugated sample (CP), Kaolin (BiP Kaolin, Denain-Anzin-Minéraux) suspensions were prepared by grinding kaolin particles in water with a dispersant (Dolaflux; 0,2wt%) in a planetary mill (Fritsch, Pulverisette, during 40 min at 180 rpm). The suspensions were placed in a cylindrical container to operate centrifugation. The container axis was placed perpendicular to the centrifugation axis (Fig. 1a), resulting in disc-shaped samples (36 mm × 1-5 mm) having their revolution axis perpendicular to the axis of rotation of the centrifugation machine (Sigma 301). Centrifugation was operated up to obtain a density equilibrium, defined by a constant thickness of the powder compact, and results in a quasi-uniaxially applied pressure σ along the containner axis, which depends on many factors [12]. Sample CP was elaborated using a suspension height before centrifugation in the container of 14.9 mm. The centrifugation was operated in three successive stages: (i) centrifugation at 3000 rpm during 20 min; (ii) water excess removal and (iii) centrifugation at 3600 rpm during 10 min. Raw disks were then dried between 2 flat and porous materials to sinter them using a 5°C/min heating rate and a maximum temperature of 1410°C maintained during 2h. For the uniaxially pressed composite sample (UP, Fig. 1b), large $2M_1$ muscovite flakes (20-50mm) from Bihar (India) [13] and very high purity Kaolinite (reference material kga-1b from the Clay Mineral Society, University of Missouri, USA) were used. Kaolinite was deposited on muscovite flakes using a concentrated aqueous suspension (40vol%) obtained by ball grinding the kaolinite powder in water [14]. After kaolinite deposition, the obtained layers were stacked under uniaxial load and the resulting sample dried at 100°C during 2h. The sintering cycle was optimised in order to overcome as much as possible porosity development due to muscovite dehydroxylation. Sintering kinetics control under uniaxial load above 1100°C where significant densification is observed helped in this optimisation [14].

The aggregate contains as major phase montmorillonite, and cristobalite/tridymite interlayer structure (opal CT) and quartz as minor phases, all in amounts to determine. This material is a standard montmorillonite clay from the American Clay Society, STx-1 Ca-montmorillonite from Texas [15], with a grain size of 1–2 μm. The sample was prepared using a cold pressing method using uniaxial compression of the powder with a piston in a cylinder at 10 MPa for 7 days. Final sample porosity is of 36.5 vol% for a bulk density of 1.36 g/cm^3 [16].

Combined Analysis Characterisation. To characterize crystal orientation of the mullite samples, Quantitative Texture Analysis (QTA) was performed using a 4-circle diffractometer allowing rapid acquisition of the whole diffraction pattern up to 80° 2θ in the reflection mode, for each tilt angle χ and azimuth angle φ of the samples orientation. Diagrams were acquired for many sample orientations (using a 5°x5° measuring grid in (χ,φ) up to χ=55°). When smooth enough texture was observed data were binned to a 15°x15° grid for subsequent treatments. For the phyllosilicate, the transmission geometry and a 2D image plate detector (MAR345) were used at the BESSRC 11-ID-C high-energy synchrotron beamline of the Advanced Photon Source at Argonne National Laboratory, using a wavelength of 0.107877 Å. This sample was assumed having a fibre-like texture because of uniaxial pressing, and in this case a single image is enough to completely determine the

texture. The image was divided in 36 10°-angular sectors to construct as many diagrams for the analysis [16]. In all samples the whole dataset was then analyzed using Whole-Powder-Pattern Rietveld analysis within the Combined Analysis formalism [17], in which the orientation distribution function (ODF) was refined either using the E-WIMV approach [18] for the mullite samples or standard functions [19] for the montmorillonite. Briefly, Combined Analysis uses the y_{ic} calculated intensity profile of each diagram measured at point i (i = 2θ or any other variable), under (χ,φ) and an incident angle ω, to extract integrated intensities:

$$y_{ic}(\omega,\chi,\varphi) = y_{ib}(\omega,\chi,\varphi) + \sum_{\Phi=1}^{N_\Phi} S_\Phi \sum_{k=K_1}^{K} j_{\Phi k} Lp_{\Phi k} P_{\Phi k}(\omega,\chi,\varphi) |F_{\Phi k}|^2 \Omega_{i\Phi k} A_{i\Phi}(\omega,\chi,\varphi) \quad (1)$$

This profile is compared to the observed y_{io} profile, and the calculated diagrams are adjusted to observations using for instance a non-linear least-squares minimisation technique. In this equation the various variables are:

- $j_{\Phi k}$ the multiplicity factor of the peak for phase Φ
- $Lp_{\Phi k}$ the Lorentz-polarisation factor
- $P_{\Phi k}$ the correction factor describing preferred orientations of phase Φ
- $|F_{\Phi k}|$ the modulus of the structure factor (including thermal vibrations) of phase Φ
- $\Omega_{i\Phi k}$ the profile function of the peaks of phase Φ, which represents instrumental and potential sample broadenings due to crystallite finite sizes and microstrains
- $A_{i\Phi}$ the absorption factor which takes into account the experimental and sample geometries.

Preferred orientation (Texture) factors entering each diagram are obtained from integrated intensities. These latter are extracted using the texture-adapted Le Bail approach [20], a way of obtaining integrated intensities of individual reflections k from powder diagrams exhibiting a lot of overlaps:

$$I_{o,k} = \sum_i \frac{(y_{io} - y_{ib}) W_{ik} I_{c,k}}{(y_{ic} - y_{ib})} \quad \text{with} \quad y_{ic} = \sum_k W_{ik} I_{c,k} \quad (2)$$

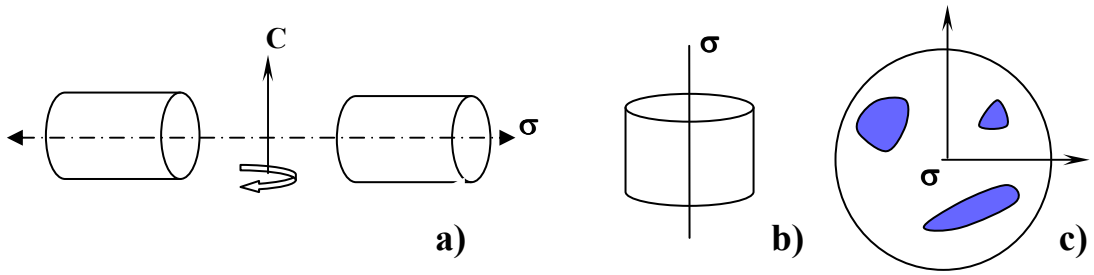

Figure 1: Configurations of sample loads for **a)** centrifugation, **b)** uniaxial pressure, and **c)** corresponding pole figure frame

In Equation (2), W_{ik} takes into account all other factors like scale, multiplicity of the line, Lorentz-polarisation factors, peak-shape function ..., and $I_{c,k}$ is calculated from the initial ODF. The initiated $I_{c,k}$ values are forced to the same weight, i.e. 1 (randomly oriented sample). In the following cycles, the $I_{o,k}$ values previously obtained are substituted to the $I_{c,k}$ of the decomposition formula. During the iterations the least-squares procedure then forces the respective intensities to become coherent with the observed overlap, and progressively converge to the observed intensities. The extracted intensities are then finally obtained directly from the observation best fit, and serve texture factor for next ODF refinements.

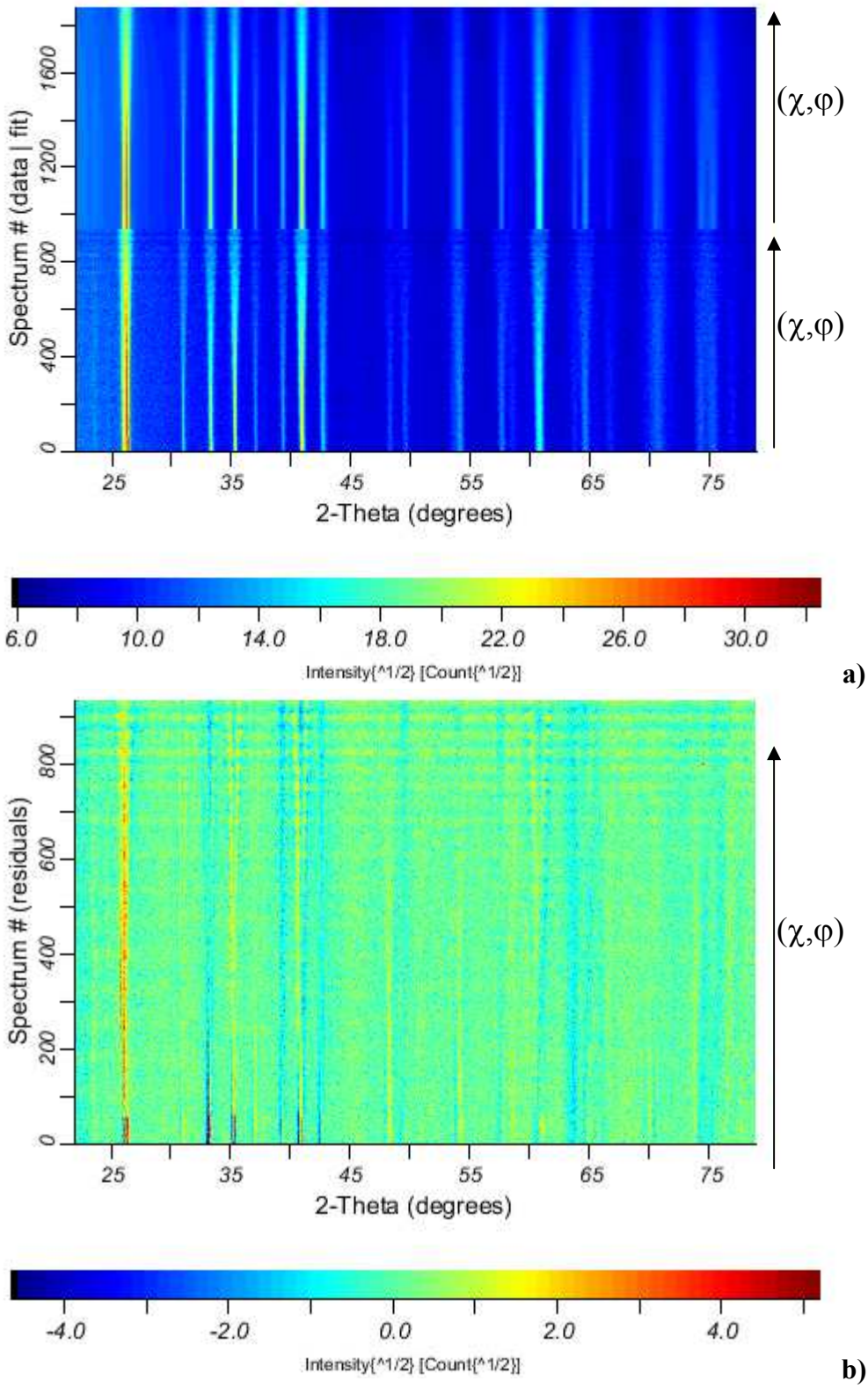

Figure 2: Typical reproducibility of the refinement illustrated on the **a)** 936 experimental (bottom set) and refined (Top set) diagrams of a mullite ceramic sample and **b)** difference between experiments and refinements. The diagrams are developped in (χ,φ) on the vertical axis.

Pole figures obtained from the resulting ODF are plotted using an equal area projection on the sample disc plane, with their centre being the **σ** direction (Fig. 1a-c), and are normalized into distribution densities using multiple of a random distribution (m.r.d.) units. Using such units, a sample without texture exhibits homogeneous pole figures with 1 m.r.d. values, while a textured

sample shows minima and maxima in the pole figures ranging from 0 m.r.d. (absence of crystals oriented in this direction) to infinity (for a single crystal on few directions).

The overall texture strength is evaluated through the texture index [21]. The normalization of the pole figures into m.r.d. values is operated during the orientation distribution (ODF) refinement of crystallites during the E-WIMV step. The ODF and profile refinement reliabilities are estimated using conventional reliability factors [22].

Uniaxially pressed mullite

Under optimized conditions, dense and well-crystallized materials are obtained showing typical in-plane crossed-needles (Fig. 3a) with mullite acicular crystals forming roughly triangular and interpenetrated nets, perpendicularly to **σ** as expected from this anisotropic shape. With Bi_2O_3 addition, a less organised microstructure is observed [14].

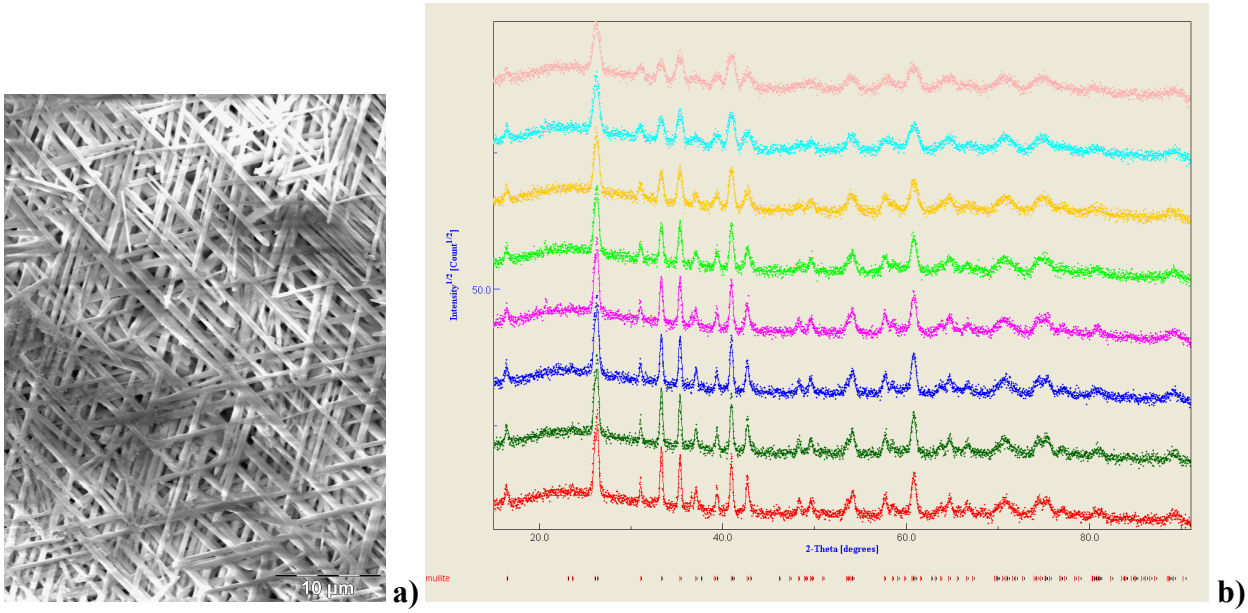

Figure 3: a) SEM image of a kaolinite-muscovite composite sintered at 1250°C without Bi_2O_3 addition, and **b)** corresponding set of x-ray patterns measured at increasing χ-values (from bottom to top)

Combined analysis (Fig. 3b) practiced on the UP sample reveals that the only phases present in the sample are mullite and an amorphous phase that could be fitted using amorphous silica. The fit quality is obtained with good reliability factors of R_w = 4.87 % and R_B = 4.01 % for the ODF refinement, and R_w = 12.90 % and R_B = 10.28 % for the Rietveld fit, giving an overall goodness of fit of 1.77. The refined cell parameters are similar to that of mullite (a = 7.56486(5) Å; b = 7.71048(5) Å; c = 2.89059(1)Å) as determined by other authors [23, 24]. The {020}, {200} and {001} pole figures for the main indices of this sample (Fig. 4a), show as a main texture component a planar texture with <001> directions aligned roughly at random in the sample plane, *i.e.* perpendicular to the pressure axis, all other crystallographic directions being at random around the c-axes. Another minor preferred orientation component is seen in the centre of the {200} pole figure, indicating a fibre texture with a-axes of mullite defining the fibre axis perpendicular to the sample plane. The two texture components achieve a maximum of 1.8 m.r.d. on the {200} pole figure and around 1.39 m.r.d. at the periphery of the {001} pole figure, with an OD texture index of 1.2 m.r.d.^{2} revealing the overall weakly stabilised texture strength. Looking closer at the {001} pole figure (Fig. 4b) one can identify a series of six {001} poles located at approximately χ=60° each

other around the sample normal, as a sign of a subsidiary organization of the c-axes in the sample plane. On this figure the 0.68 minimum density indicates that 68% of the crystals are not oriented with their c-axes corresponding to the mean orientation component. These pole reinforcements are to be correlated with the triangular network seen on SEM images, and are coherent with long mullite crystal axes corresponding to <001>.

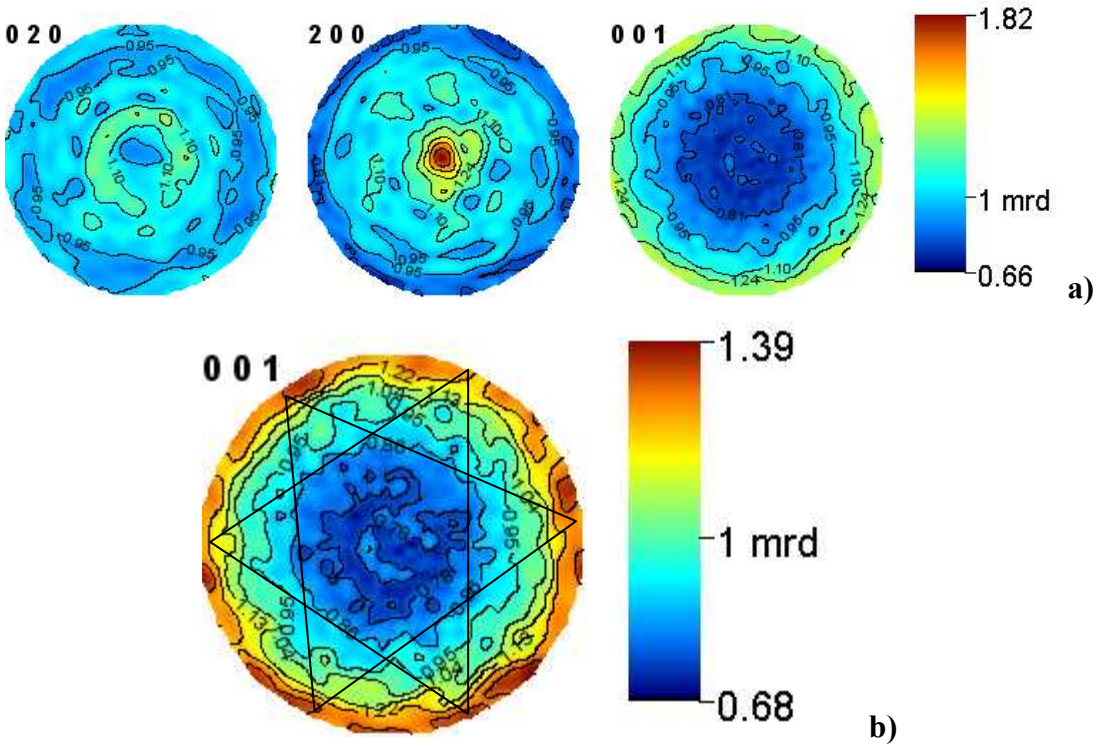

Figure 4: a) Recalculated-normalised {020}, {200} and {001} pole figures for the main axes of mullite. **b)** {001} pole figure represented to show the pole reinforcements linked to the in-plane triangular-like organization of the mullite needles (Figurea). Linear density scales.

Centrifugated mullite-silica composite

Using centrifugation, the process needs to be optimised with concerns on porosity, density, and mechanical behaviour, by varying temperature and suspension height in the container [12]. We illustrate here QTA results on a sample elaborated with a suspension height of 9.8 mm at a temperature of 1410°C, with as only crystalline phase the (3:2) mullite, in an amorphous phase. Considering that the amorphous phase is similar to amorphous silica (refined to 24.4 % in weight, with a unit-cell parameter of 6.931(3) Å and a mean crystallite size of 10.38(3) Å), the fit quality is obtained with good reliability factors (R_w = 11.8 %, R_B = 9.3 %, GoF = 1.1 for the Rietveld fit, R_w = 5.7 %, R_B = 5.6 % for the ODF). As for the UP sample, the refined cell parameters are in good agreement with the ones of mullite from literature, with a = 7.51996(6) Å; b = 7.66161(5) Å; c = 2.87591(1)Å.

The {001} pole figure (Fig. 5) shows the distribution of c-axes at random in the sample plane, as in a so-called "planar texture". The maximum orientation density is then located at the periphery of the {001} pole figure and reaches 1.56 m.r.d.. The corresponding OD texture index is of 1.14 m.r.d^2, revealing the overall weakly stabilized texture strength, but similar to the UP sample. The planar texture corresponds to a realignment of the c-axes perpendicularly to the pressure direction of centrifugation (σ), which allows the association of mullite needle main axes to the

crystallographic c-axes. A small tilt angle is seen for this sample, due to the specificity of the centrifugation process. Most importantly, the minimum value of the {001} pole figure indicates that still nearly 60% of the volume of the sample is not oriented within this texture component.

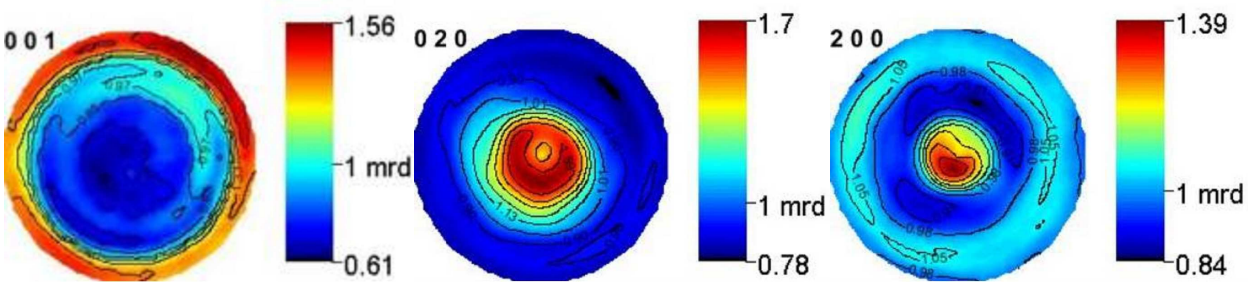

Figure 5: {001}, {020} and {200} pole figures of mullite of the 9.8 mm centrifugated samples

Around the c-axes, all other crystallographic directions are randomly distributed for a planar texture. Consequently, a broad maximum should be observed in the center of any {hk0} pole figure, like {020} or {200} (Fig. 5), which indeed appear with a maximum of 1.7 m.r.d. and 1.39 m.r.d. respectively. However, one can see that the {200} pole figure is not fully respecting this scheme, but also exhibit a reinforcement near its equator, superposed to the planar component at its centre. This is coherent with the existence of a second texture component, corresponding to a <010> fibre-like texture. This latter component looks to increase with the initial suspension height [12].

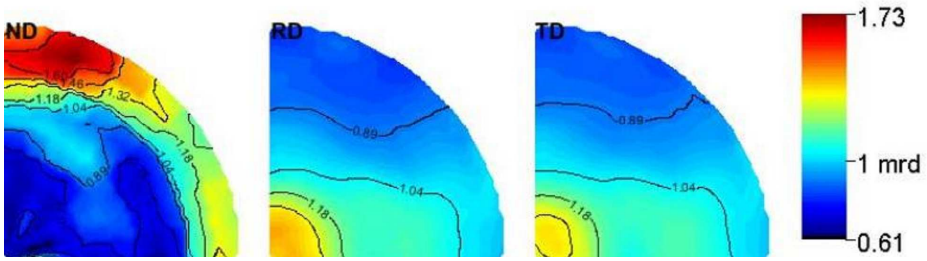

Figure 6: Inverse pole figures recalculated from the ODF for the **σ** (ND), **x** (RD) and **y** (TD) centrifugated sample directions

The proportion of each of the texture components is best appreciated on inverse pole figures (Fig. 6) plotted for the main sample directions, **σ** (ND), **x** (RD) and **y** (TD). In the **σ** inverse pole figure, one can clearly see the broad periphery corresponding to all <hk0> contributions to the planar texture component. Simultaneously, a relatively strong <001> direction pole is observed on the **x** and **y** inverse pole figures corresponding to the homogeneously distributed c-axes in the sample plane. The minimum ODF in this sample indicates that still 41 % of the sample volume corresponds to randomly oriented crystals.

The centrifugation process can then exhibit reasonably good capabilities to orient mullite needles in materials from clay mineral suspensions, at least at levels comparable to the ones induced using moderate uniaxial pressures.

Phyllosilicate aggregate

A turbostratic disordered phyllosilicate aggregate containing quartz, opal-CT and cristobalite showed a prominent texture of the montmorillonite phase. Both opal-CT and monmorillonite

exhibit turbostratic character. In such disordered structures, it does not exist any regularity (either in rotation or translation) of the layers stacking, which gives rise to large and asymmetric diffraction bands (Fig. 7a). Using for both phases a supercell model of 10 unit-cells [11] to describe layer disordering along their c-axes, a good refinement is obtained (R_w = 2.08 %, R_B = 2.88 %, GoF = 3.31). In this case, the texture was simulated using a standard Gaussian component representing the cyclic-fibre texture of the montmorillonite phase (Fig. 7b). The texture strength of montmorillonite remains low, with only 1.3 m.r.d. at maximum of the {001} pole figure, and 0.85 m.r.d. at minimum. This latter value indicates a relatively large volume amount of crystallites randomly oriented in the aggregate, in coherence with the relatively low magnitude of the applied pressure.

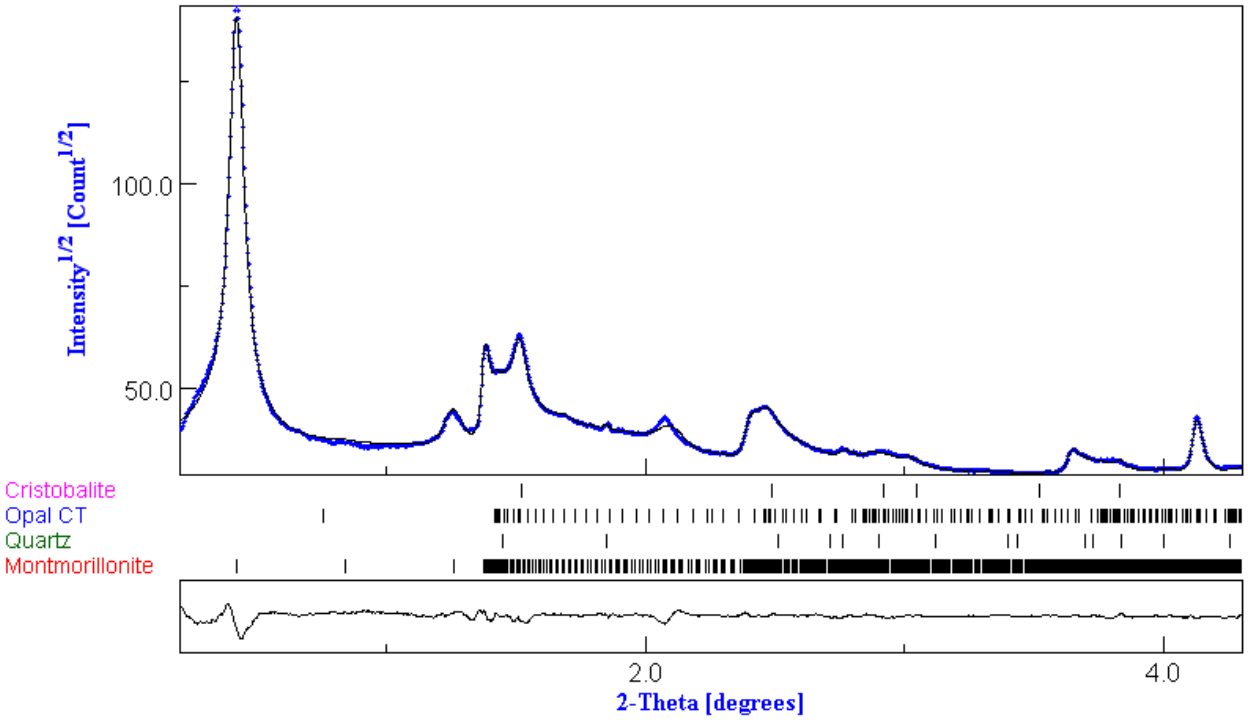

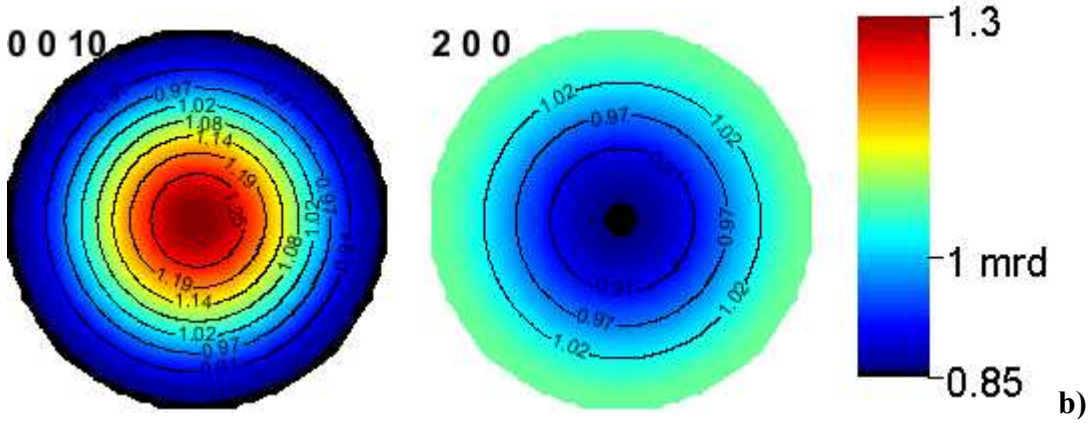

Figure 7: a) Refinement of the phyllosilicate aggregate containing two turbostratic disordered phases simulated using supercell modelling [11]. **b)** {0010} and {200} pole figures of the montmorillonite phase.

We obtained the following cell parameters for the montmorillonite: with a = 5.181(3) Å; b = 9.010(4) Å; c = 15.046(8)Å and β = 101.55(2)°; for quartz: a = 4.922(3) Å and c = 5.396(5) Å; for opal-CT: a = 5.027(3) Å and c = 8.208(4) Å; for cristobalite: a = 7.028(3) Å. All these parameters

are in good agreement with literature data. The relative phase amounts 91.8(3)%, 0.19(1)%, 6.6(1)%, 1.45(2)% respectively for montmorillonite, quartz, opal-CT and cristobalite.

Conclusions

This work shows that the orientation of mullite needles in composite ceramics is efficiently characterised using the Combined Analysis approach, even with an amount around 24wght% of an amorphous phase. Low level of texture are achieved for the cristallised mullite using moderate uniaxial pressures or centrifugation, and several texture components are stabilised. These components divide into fibre- and planar-like textures. In the phyllosilicate aggregate containing four phases, two of which being turbostratically disordered, the usual phyllosilicate asymmetric "hk" bands are correctly reproduced using a single layer model with the help of a supercell description along the stacking sequence, together with quantitative texture analysis.

Acknowledgements

The authors wish to express their gratitude to the European Community (European Social Fund and FEDER), the Limousin and Basse-Normandie Regions for financial supports to this work. We are appreciative for access to beamline 11-ID-C at APS. This research was supported by NSF (EAR-0836402) and DOE (DE-FG02-05ER15637).

References

[1] Suzuki T.S., Uchikoshi T., Okuyama H., Sakka Y. and Hiraga K.: Journal of the European Ceramic Society **26** (2006) 661–665
[2] Kim D.-K. and Kriven W.M.: Composites Part B Engineering **37(6)** (2006) 509–514
[3] Gridi-Bennadji F., Beneu B., Laval J.-P. and Blanchart P.: Applied Clay Science **38(3-4)** (2008) 259-267
[4] Lee W.E., Souza G.P., McConville C.J., Tarvornpanich T. and Iqbal Y.: Journal of the European Ceramic Society **28** (2008) 465–471
[5] Soro N., Aldon L., Jumas J.C. and Blanchart P.: Journal of the American Ceramic Society **86(1)** (2003) 129-134
[6] Pialy P., Tessier-Doyen N., Njopwouo D. and Bonnet J.-P.: Journal of the European Ceramic Society **29(9)** (2009) 1579-1586
[7] Schneider H. and Eberhard E.: Journal of the American Ceramic Society **73(7)** (1990) 2073–2076
[8] Carbajal L., Rubio-Marcos F., Bengochea M.A. and Fernandez J.F.: Journal of the European Ceramic Society **27** (2007) 4065–4069
[9] Tucci A., Esposito L., Malmusi L. and Rambaldi E.: Journal of the European Ceramic Society **27(2–3)** (2007) 1875–1881
[10] Kong L.B., Zhang T.S., Ma J. and Boey F.: Journal of Alloys and Compounds **359(1-2)** (2003) 292-299
[11] Ufer K., Roth G., Kleeberg R., Stanjek H., Dohrmann R. and Bergmann J.: Zeitschrift für Kristallographie **219** (2004) 519-527
[12] Deniel S., Tessier-Doyen N., Dublanche-Tixier C., Chateigner D. and Blanchart P.: To appear Journal of the European Ceramic Society (2010)
[13] Klein H.H., Stern W.B. and Weber W.: Schweizerische Mineralogische und Petrographische Mitteilungen **62(1)** (1982) 145-173
[14] Gridi-Bennadji F., Chateigner D., Di Vita G. and Blanchart P.: Journal of the European Ceramic Society **29(11)** (2009) 2177-2184

[15] Dähn R., Scheidegger A.M., Manceau A., Schlegel M., Baeyens B., Bradbury M.H. and Morales M.: Geochimica & Cosmochimica Acta **66** (2002) 2335-2347
[16] Lutterotti L., Voltolini M., Wenk H.-R., Bandyopadhyay K. and Vanorio T.: American Mineralogist **95** (2010) 98–103
[17] Chateigner D.: *Combined Analysis* (Wiley-ISTE, 2010). 420 pp, ISBN: 978-1-84821-198-8
[18] Lutterotti L., Matthies S. and Wenk H.-R.: National Research Council of Canada, Ottawa 1999, 1599-1604
[19] Matthies S., Vinel G.W. and Helming K.: *Standard distributions in texture analysis* Matthies (Ed.). (Akademie-Verlag Berlin, 1987), vol 1, 449p
[20] Le Bail A.: Powder Diffraction **20** (2005) 316-326
[21] Bunge H.-J. and Esling C.: *Quantitative Texture Analysis.* Bunge and Esling (Eds.) (DGM, Germany, 1982) 551 pp
[22] Chateigner D.: Journal of Applied Crystallography **38** (2005) 603-611
[23] Fischer R.X., Schmucker M., Angerer P. and Schneider H.: American Mineralogist **86** (2001) 1513-1518
[24] Gražulis S., Chateigner D., Downs R.T., Yokochi A.F.T., Quirós M., Lutterotti L., Manakova E., Butkus J., Moeck P. and Le Bail A.: Journal of Applied Crystallography **42(4)** (2009) 726-729 Crystallography Open Database n°9005501. www.crystallography.net